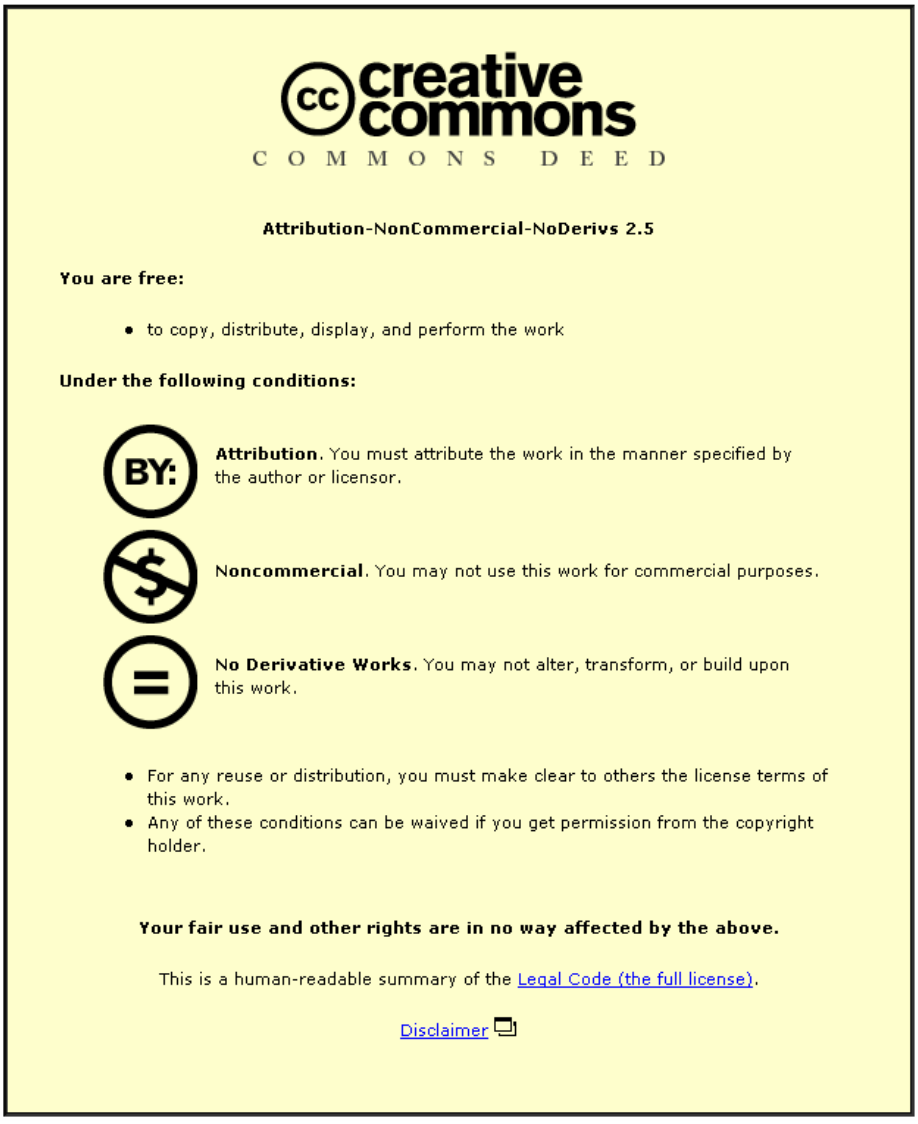

creative commons

COMMONS DEED

Attribution-NonCommercial-NoDerivs 2.5

You are free:

- to copy, distribute, display, and perform the work

Under the following conditions:

BY: **Attribution**. You must attribute the work in the manner specified by the author or licensor.

Noncommercial. You may not use this work for commercial purposes.

No Derivative Works. You may not alter, transform, or build upon this work.

- For any reuse or distribution, you must make clear to others the license terms of this work.
- Any of these conditions can be waived if you get permission from the copyright holder.

Your fair use and other rights are in no way affected by the above.

This is a human-readable summary of the Legal Code (the full license).

Disclaimer

Rotational, Vibrational, and Excitation Temperatures of a Microwave-Frequency Microplasma

Felipe Iza, *Student Member, IEEE,* and Jeffrey A. Hopwood, *Member, IEEE*

***Abstract*—Integration of microplasma sources in portable systems sets constraints in the amount of power and vacuum levels employed in these plasma sources. Moreover, in order to achieve good power efficiency and prevent physical deterioration of the source, it is desirable to keep the discharge temperature low. In this paper, the thermal characteristics of an atmospheric argon discharge generated with a low-power microwave plasma source are investigated to determine its possible integration in portable systems. The source is based on a microstrip split-ring resonator and is similar to the one reported by Iza and Hopwood, 2003. Rotational, vibrational, and excitation temperatures are measured by means of optical emission spectroscopy. It is found that the discharge at atmospheric pressure presents a rotational temperature of ∼300 K, while the excitation temperature is ∼0.3 eV (∼3500 K). Therefore, the discharge is clearly not in thermal equilibrium. The low rotational temperature allows for efficient air-cooled operation and makes this device suitable for portable applications including those with tight thermal specifications such as treatment of biological materials.**

***Index Terms*—Excitation temperature, microplasma, microwave plasma, rotational temperature, split-ring resonator, vibrational temperature.**

I. Introduction

THERE IS A growing interest in microplasma sources that can be integrated in portable devices for applications such as bio-MEM's sterilization, small-scale materials processing, and micro chemical analysis systems. Portable operation of microplasma sources, however, places a limit on the amount of power and the vacuum levels that can be employed, as well as on the maximum temperature the discharge can reach.

For portable applications it is desirable to operate the discharges at atmospheric pressure since this eliminates the need for vacuum pumps. Micropumps increase the final cost of the system, are inefficient in achieving high vacuum levels, and may reduce the overall system reliability. The temperature of the atmospheric discharge, however, should remain low to prevent erosion and melting of the source. Given the small dimensions of these devices, even damage on the order of microns, that could be tolerated in large-scale sources, may become catastrophic and make the microdevice inoperable in short periods of time [1].

Operation at atmospheric pressure has been achieved with a variety of microfabricated plasma sources. The dc sources [1], [2] are simple to fabricate but present a limited lifetime due to sputter erosion of the microelectrodes. This electrode erosion has been exploited, however, to detect metals using microfabricated liquid electrodes [3]. Microhollow cathodes operating at high pressure have also been investigated. They typically produce intense discharges rich in UV radiation [4], [5]. These discharges, however, exhibit discharge (gas) temperatures in the order of thousands of Kelvin [6], which limits their lifetime and their application in portable devices. Dielectric barrier discharges (DBD) are also the subject of intense research for their simplicity and extensive use in plasma displays [7]. Dielectric and resistive barrier, as well as corona discharges, are also being investigated for use in biological and environmental applications [8]–[10]. Sources operating with radio-frequency (RF) power at atmospheric pressure have also been investigated. Examples of these are the capacitively coupled plasma source [11] and the plasma needle [12]. Plasma sources operating at microwave frequencies and atmospheric pressure have also been miniaturized [13]–[15].

It was suggested in [15], that the discharge obtained by a low-power microwave plasma source based on a split-ring resonator remained cool at atmospheric pressure. This paper studies the thermal characteristics of a discharge generated with a similar device. This microplasma source differs from that reported earlier [15] in that the matching network has been eliminated and the discharge gap size has been reduced from 500 to 120 μm. These modifications result in a more compact design with improved performance at high pressures.

Rotational, vibrational, and excitation temperatures have been measured by means of optical emission spectroscopy for pressures varying from 1 torr (133 Pa) to atmospheric pressure. The spectrum analysis shows that the discharge presents an excitation temperature of ∼0.35 eV and that the population of the vibrational states and the excited atomic levels for an atmospheric discharge presents an overpopulation of low-energy levels. The rotational temperature at atmospheric pressure is ∼300 K which agrees with the initial observations reported in [15].

II. Experiment

A. Microplasma Generator

The plasma source used in this paper consists of a microstrip split-ring resonator as shown in Fig. 1. The ring resonator is a half wavelength in circumference, and it is in the small gap of the split-ring resonator that the plasma is ignited. The maximum voltage difference in the device occurs across the gap,

Manuscript received August 28, 2003; revised October 10, 2003. This work was supported in part by the National Science Foundation under Grant DMI-0078406. The work of F. Iza was supported in part by the Fulbright Program.

The authors are with the Electrical and Computer Engineering Department, Northeastern University, Boston, MA 02115 USA (e-mail: hopwood@ece.neu.edu).

Digital Object Identifier 10.1109/TPS.2004.826145

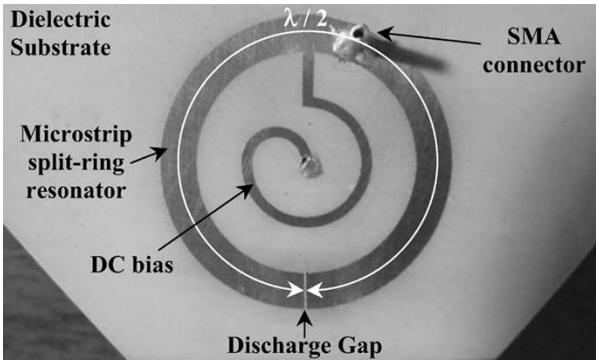

Fig. 1. Picture of the microwave plasma source. Top view of the microstrip structure. Frequency of operation ∼825 MHz.

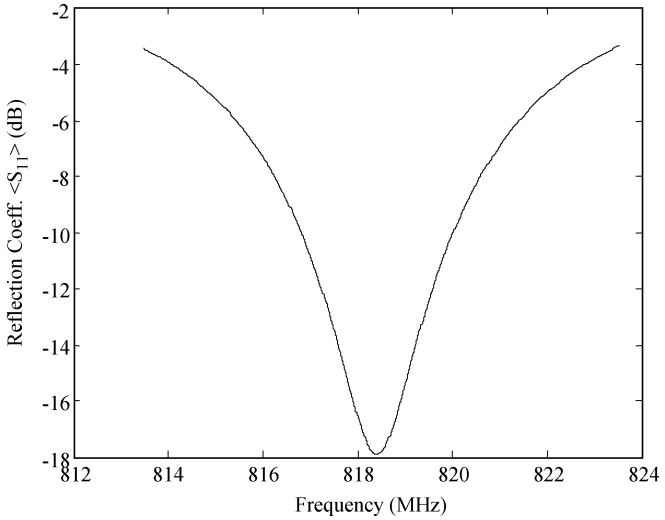

Fig. 2. Reflection coefficient (S_{11}, in decibels) measured with a HP8714ET network analyzer.

favoring the discharge breakdown in this region, while minimizing losses in the rest of the device [15]. Although unnecessary for its operation, an additional quarter-wave structure has been added in the center of the ring to dc bias the resonator. This central, spiral-shaped transmission line is electrically grounded so that the resonator's microstructure has a well-defined dc potential (0 V).

The device was fabricated on RT/Duroid 6010.8 laminate, which consists of a 635-μm-thick dielectric coated with 9-μm -thick copper on both sides. The dielectric material is made out of ceramic-reinforced teflon with a relative dielectric constant of 10.8. The microstrip pattern is transferred using photolithography and wet etching techniques, and a subminiature type A connector (SMA) is attached perpendicular to the microstrip to deliver power to the plasma generator. The power is directly coupled into the resonator at a point on the ring where the input impedance of the resonator matches that of the power supply (50 Ω). This eliminates the need for matching networks, such as those used in other microfabricated microwave plasma sources [13]–[15], resulting in a more compact design without sacrificing performance.

Fig. 2 shows the reflection coefficient (S_{11}) of the device (including the SMA connector) measured with a HP-8714ET network analyzer. From the reflection coefficient, a measure of the

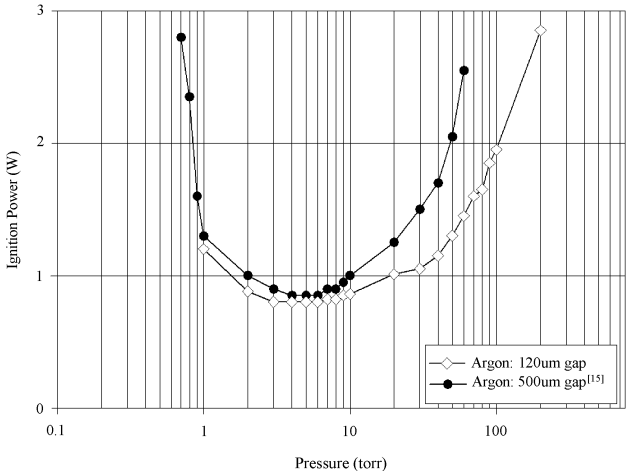

Fig. 3. Ignition power versus pressure for argon.

quality factor of the device can be obtained as $f_c/\Delta f_{3\ dB}$, where f_c is the resonant frequency and $\Delta f_{3\ dB}$ the bandwidth where the reflection coefficient increases by 3 dB from its value at resonance [16]. From Fig. 2, the ratio $f_c/\Delta f_{3\ dB}$ for the device is ∼480, which is of the same order of magnitude than that of a previous microwave source based on a split-ring resonator [15].

The plasma source has a gap size of 120 μm. As long as the coupling between the two ends of the resonator is negligible, a smaller gap size produces a higher electric field in the gap region for the same input power. A higher electric field provides better performance particularly at high pressure. Fig. 3 shows the power needed to ignite an argon discharge as a function of pressure and compares it with a similar device with a wider gap (500 μm) [15]. A minimum in the ignition power occurs around 5 torr (666.4 Pa), the pressure at which the power absorbed by the plasma is maximum for a given electric field (i.e., $\omega = \nu$ [17], where ω is the frequency of excitation and ν the electron collisional frequency). The advantage of the increase in electric field strength afforded by the smaller gap is clearly evident in Fig. 3. At higher pressures, the plasma ignites at lower power.

B. Experiment Setup

Once the device has been fabricated and the SMA connector bonded, it is attached to a glass tube that acts as a vacuum chamber. The glass tube is terminated in a metal flange that attaches the tube to a vacuum manifold (see [15, Fig. 4] for a schematic of a similar experiment setup).

The gases used for the experiments are high purity argon and nitrogen, and a mechanical pump is used to create vacuum in the chamber when needed. A capacitance manometer measures the pressure in the chamber and a needle valve at the inlet allows one to vary the pressure by altering the gas flow. For pressures higher than 10 torr (1.33 kPa), a calibrated convectron pressure gauge is used to measure the gas pressure.

A signal generator (HP-8656A) and a 3 W linear RF amplifier (ENI-603L) are used to supply power to the plasma source. A dual directional coupler and a RF power meter are used to measure the forward and reflected power. In this paper, the plasma power is reported as the difference between the forward and reflected power.

The optical emission from the plasma is collected using a 20-mm-diameter lens placed next to the discharge. The collected light is focused into a quartz optical fiber bundle and transmitted to a Jarrel–Ash diffraction grating monochromator. An optical multichannel analyzer (OMA) consisting of a 1024 pixel Si-photodiode array detector (EG&G 1453A) and a controller (EG&G 1451) is used to record the emission spectra. The OMA can detect light emission with wavelengths in the range of 3000 to 10 000 Å, and the optical transmission as a function of wavelength has been corrected using a calibrated optical power meter.

III. Temperature Determination From Optical Emission

Optical emission spectroscopy is particularly convenient for the study of microdischarges since Langmuir probe measurements are unreliable given the size of the discharge. It is also a nonintrusive and inexpensive means to determine the various temperatures in the discharge by analyzing line and band emission intensities.

The split-ring resonator discharge is not in thermal equilibrium and, therefore, different temperatures can be defined to characterize the electron energy distribution (electron temperature), the population of atomic excited states (excitation temperature), and the population of vibrational and rotational molecular states (vibrational and rotational temperature).

Inherent in all the temperature calculations is the assumption that the electron energy distribution function follows a Maxwellian distribution. In our discharge, the electron temperature ($\mathrm{T_e} \sim \mathrm{T_{exc}} \sim 1$ eV) is significantly lower than the threshold energy for excitation and ionization (11.5 eV and 15.8 eV, respectively, for argon). Therefore, one should expect a depopulation of high-energy electrons as a result of excitation and ionization processes. Nevertheless, even when electrons do not follow a Maxwellian distribution, it is still possible to calculate a temperature that fits the experimental data. One, however, should be aware of its meaning and limitations. In fact, the further one departs from the thermodynamic equilibrium condition, where all processes are in detailed balance [18], the more diffused the notion of temperature becomes. In many cases, it is necessary to define two-temperature distributions functions to better describe the population of different energy states.

Excitation and vibrational transitions are primarily dominated by electron collisions and, therefore, their populations provide some insight into the electron temperature. On the other hand, since electrons are inefficient in providing rotational energy to molecules due to their small mass, the population of rotational states is controlled by collisions with heavy particles. Therefore, the rotational temperature is an estimate of the heavy particle (gas) kinetic temperature.

A. Excitation Temperature

The excitation temperature describes the population of atomic excited states assuming that this follows a Boltzmann distribution. Taking into account the degeneracy of each atomic state, the population is given by [19, p. 191]

$$\frac{\mathrm{n_u}}{\mathrm{g_u}} = \frac{\mathrm{n_l}}{\mathrm{g_l}} \exp\left(-\frac{\mathrm{E_l} - \mathrm{E_u}}{\mathrm{k}\,\mathrm{T_{exc}}}\right) = \frac{\mathrm{n}}{\mathrm{Z}} \exp\left(-\frac{\mathrm{E_u}}{\mathrm{k}\,\mathrm{T_{exc}}}\right)$$

where $\mathrm{n_u}$ and $\mathrm{n_l}$ are the number densities of atoms in the excited levels u and l, respectively, $\mathrm{E_l}$ and $\mathrm{E_u}$ the energies of the states, $\mathrm{g_u}$ and $\mathrm{g_l}$ the statistical weights (degeneracy), k the Boltzmann's constant, n the sum of number densities in all states, Z the atomic partition function, and $\mathrm{T_{exc}}$ the excitation temperature. From the above expression, it is possible to determine the excitation temperature once the populations of two or more states are known.

The population of a state can be determined from the optical emission spectrum. Each emitted atomic line can be identified with a transition from an upper energy state u to a lower one l. The line intensity associated with the transition is proportional to the number density of atoms in the upper state, the probability of the transition (Einstein coefficient A) and the energy of the emitted photon [19, p. 281]

$$\mathrm{I_{ul}} \propto \mathrm{h}\nu_{\mathrm{ul}}\mathrm{A_{ul}}\mathrm{n_u} \propto \frac{\mathrm{h}}{\lambda_{\mathrm{ul}}}\mathrm{A_{ul}}\mathrm{g_u} \exp\left(-\frac{\mathrm{E_u}}{\mathrm{k}\,\mathrm{T_{exc}}}\right)$$

where his Planck's constant, ν_{ul} the frequency of the emitted photon, λ_{ul} the wavelength of the emitted photon, $\mathrm{A_{ul}}$ the Einstein coefficient, and $\mathrm{n_u}$ the number density of atoms in the excited state u. Therefore, the slope of a plot of the natural logarithm of "$\mathrm{I_{ul}}\lambda_{\mathrm{ul}}/(\mathrm{g_u}\mathrm{A_{ul}})$" versus the energy of the upper state of the transition $(\mathrm{E_u})$ is inversely proportional to the excitation temperature. Such a plot is referred as a Boltzmann plot. The data (wavelengths, energies, statistical weights, and transitions probabilities) of the observed argon lines used in this paper were obtained from [20].

B. Vibrational Temperature

The vibrational temperature describes the population of the vibrational states of molecular species. As in the case of excitation temperature, the population is assumed to follow a Boltzmann distribution and the same procedure is followed to determine the vibrational temperature. In this case, however, the Frank–Condon factors for vibrational transitions replace the Einstein coefficients and are used to construct the Boltzmann plot. Since argon is an atomic gas, a 0.1% trace of nitrogen was introduced in the discharge and the vibrational temperature of the nitrogen determined. Because pure vibrational transitions emit in the infrared and cannot be detected by the silicon OMA detector, the first and second positive systems of nitrogen ($\mathrm{B^3\Pi_g} \rightarrow \mathrm{A^3\Sigma_u^+}$ and $\mathrm{C^3\Pi_u} \rightarrow \mathrm{B^3\Pi_g}$, respectively) that emit within the spectral detection band have been used for this calculation. The sequences $\Delta\nu = -1, \ldots, -4$ of the first positive system and $\Delta\nu = 0, \ldots, 5$ of the second positive system have been used for this calculation, where $\Delta\nu$ indicates the difference in the vibrational quantum number ν of the energy levels involved. Overlapping transitions have been disregarded for the calculation and band-head wavelengths and Frank–Condon factors were obtained from [21].

C. Rotational Temperature

The rotational temperature describes the population of the rotational levels in molecular species. The distribution, unlike that of vibrational levels, is not given by a pure Boltzmann distribution. Each rotational level has a different statistical weight due

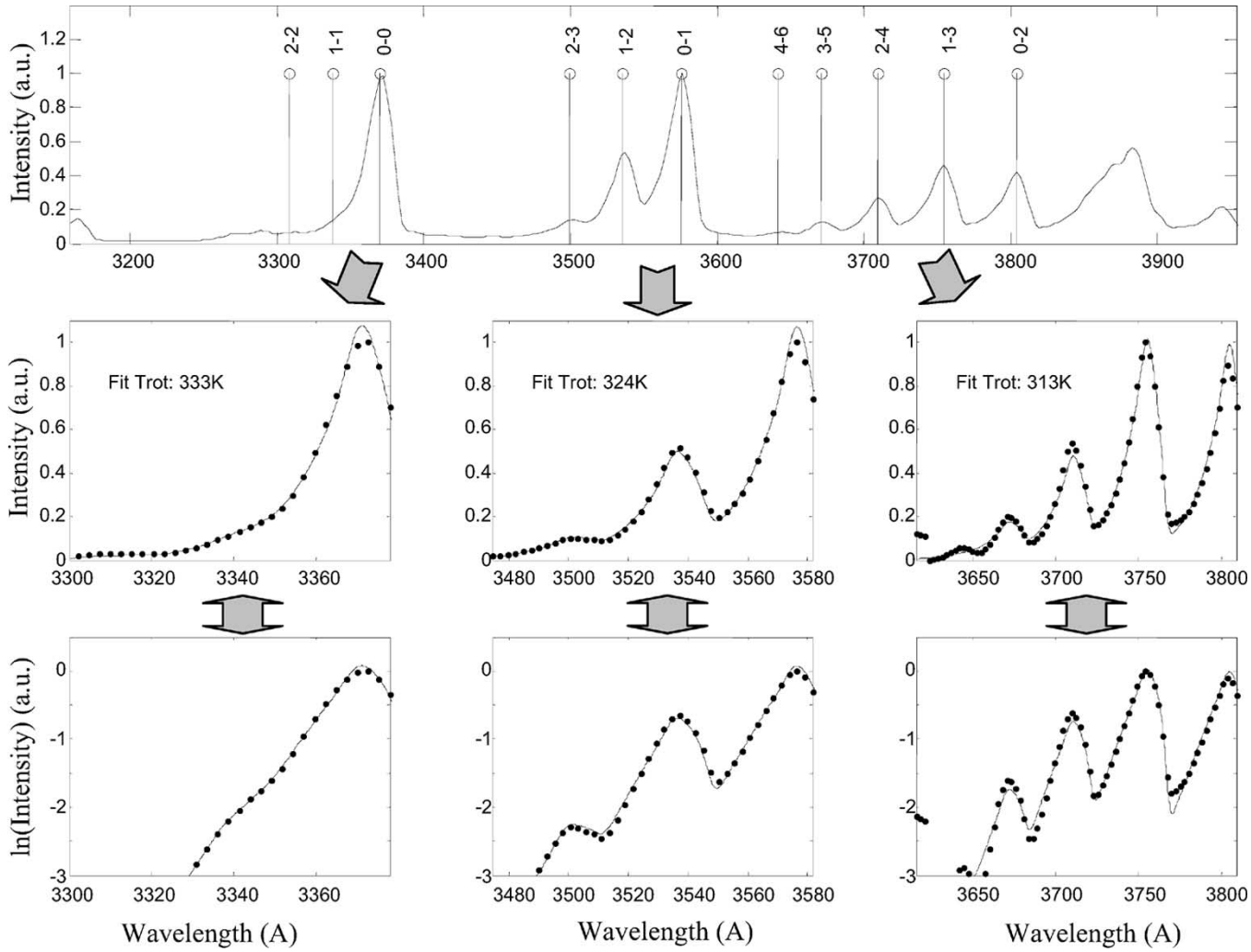

Fig. 4. Example fit of rotational temperature to experimental data. Dots: Experimental data. Solid line: Fit.

to the $(2\mathrm{J}+1)$-fold degeneracy of the states, where J is the total angular momentum of the molecule. Therefore, the thermal distribution of the rotational states will be given by the product of the Boltzmann factor $\exp(-\mathrm{E}/\mathrm{kT})$ times the statistical weight $(2\mathrm{J}+1)$ [22, p. 124].

The Jarrel–Ash monochromator used in this paper does not resolve the rotational structure, so in order to calculate the rotational temperature, we have fitted the experimental data with a theoretical calculation that takes into account the instrument line broadening of the spectrometer. The spectrum as a function of the rotational temperature is calculated using the R ($\Delta\mathrm{J}=1$), P ($\Delta\mathrm{J}=-1$) and Q ($\Delta\mathrm{J}=0$) branches of the rotational structure for each vibrational transition and then convolved with the instrument broadening function. The instrument broadening is determined experimentally from the profile of a neighboring argon atomic line (3834.7 Å). Neglecting spin splitting and Λ-doubling, the intensity of a transition from a J' state to a J'' state is given by [23, p. 127]

$$\mathrm{I}_{\mathrm{J}'-\mathrm{J}''}=\mathrm{c}\frac{\mathrm{S}_{\mathrm{J}'-\mathrm{J}''}}{\lambda^4}\exp\left(-\frac{\mathrm{E}_{\mathrm{J}'}}{\mathrm{k}\,\mathrm{T}_{\mathrm{rot}}}\right)$$
$$=\mathrm{c}\frac{\mathrm{S}_{\mathrm{J}'-\mathrm{J}''}}{\lambda^4}\exp\left(-\frac{\left(\mathrm{B}_{\mathrm{e}}-\alpha_{\mathrm{e}}\left(\nu'+\frac{1}{2}\right)\right)\mathrm{J}'(\mathrm{J}'+1)}{\mathrm{k}\,\mathrm{T}_{\mathrm{rot}}}\right)$$

where c is a constant for a given electronic+vibrational transition, $\mathrm{S}_{\mathrm{J}'-\mathrm{J}''}$ is the Hönl–London factor for the transition that accounts for the degeneracy of the states, λ the wavelength of the emitted photon, $\mathrm{E}_{\mathrm{J}'}$ the energy of the upper level of the transition, B_{e}, and α_{e} rotation molecular constants [22, p. 552], ν' and J' the vibrational and rotational quantum number of the upper state, and $\mathrm{T}_{\mathrm{rot}}$ the rotational temperature.

A rotational temperature for each of the $\Delta\nu=0$, $\Delta\nu=1$ and $\Delta\nu=2$ sequences of the second positive system ($\mathrm{C}^3\Pi_{\mathrm{u}}\rightarrow\mathrm{B}^3\Pi_{\mathrm{g}}$) has been calculated. Measured spectra and a typical numerical fit are shown in Fig. 4.

IV. Results and Discussion

A. Excitation Temperature

Fig. 5 shows the excitation temperature as a function of pressure for a 99.9% argon discharge. Excitation temperature reduces from 0.4 to 0.3 eV as the pressure is increased from 1 torr (133.3 Pa) to atmospheric pressure. These values are in agreement with the excitation temperatures reported in [12] for a low-power atmospheric argon discharge. The error bars in the figure reflect the standard deviation of the measurements. No

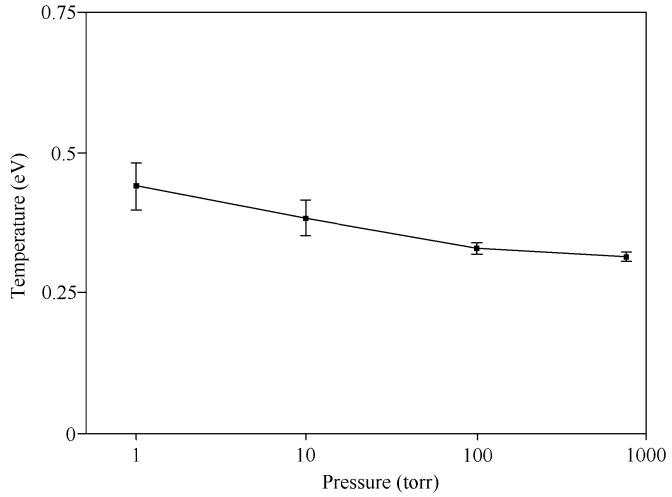

Fig. 5. Excitation temperature versus pressure for argon discharge with a 0.1% trace of nitrogen.

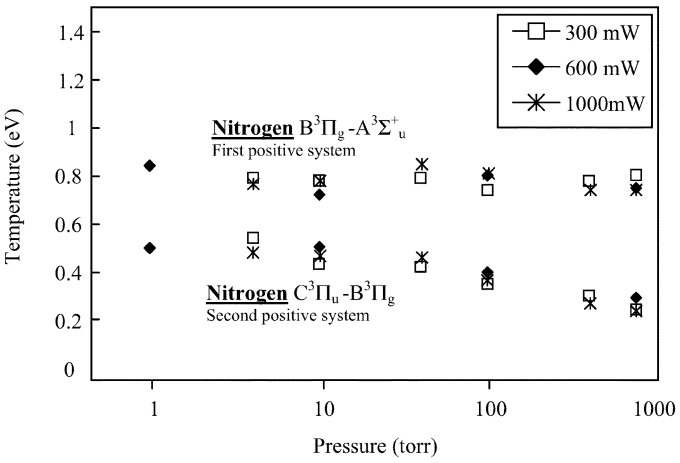

Fig. 6. Nitrogen vibrational temperature for the first and second positive systems versus pressure for a 99.9% Ar–0.1% N_2 discharge at 0.3, 0.6 and 1.0 W.

power dependence was observed when the power was varied from 0.3 to 1 W.

B. Vibrational Temperature

Excitation (Fig. 5) and vibrational (Fig. 6) temperatures present a similar trend as a function of pressure and power since both are primarily controlled by the same mechanism, i.e., electron collisions. The vibrational temperatures obtained from the first and second positive bands, however, differ significantly one from the other. This is yet another indication of the nonequilibrium condition of the discharge. Vibrational states in the lower electronic state $(B^3\Pi_g)$ present a higher vibrational temperature than the vibrational states in a higher electronic state $(C^3\Pi_u)$. The vibrational temperature obtained from the second positive system (high-energy states) is comparable with the argon excitation temperature.

Fig. 7 shows the relative population of argon and nitrogen excited states (n_u) as a function of energy with respect to the argon and nitrogen ground states for a 1 W Ar discharge at atmospheric pressure with a 0.1% trace of N_2. The relative populations of argon and nitrogen have been adjusted taking into account their different partial pressures in the discharge. The population of states resembles that of a discharge in excitation saturation balance (ESB) [18], where low-energy states are overpopulated due to the step-like ionization and excitation processes. An additional fit of the excitation temperature for argon excited levels with energies above 14 eV shows a higher excitation temperature (0.79 eV) than a fit including lower energy states (0.32 eV), which suggests that levels below 14 eV are not in Saha equilibrium [18], [23].

C. Rotational Temperature

Fig. 8 shows the rotational temperature as a function of pressure for a 99.9% Ar–0.1% N_2 discharge at different power levels. The values presented are the average values of the rotational temperatures obtained from a fit to the $\Delta\nu = 0$, $\Delta\nu = 1$, and $\Delta\nu = 2$ sequences of the second positive system of nitrogen. The standard deviation of the three numerical fits sets a maximum error of $+/-50$ K. The rotational temperature at 1 torr (133.3 Pa) and input power larger than 600 mW is not displayed because it cannot be obtained due to an impedance mismatch.

For the experimental conditions shown in Fig. 8, the rotational temperature shows no significant power dependence. Although the discharge temperature might be expected to increase with power, it is important to notice that the size of this discharge is not constrained by a plasma chamber. Therefore, as the power is increased the volume of the discharge also increases such that the power density is approximately constant. As a result, the rotational temperature does not increase with power.

As shown in Fig. 8, increasing the pressure up to 10 torr (1.3 kPa) results in an increase of the rotational temperature. This can be attributed to a higher electron-neutral collision frequency that increases the energy transfer from electrons to heavy particles. The maximum rotational temperature is obtained at 10 torr, however, any further increases in pressure result in a lower rotational temperature. This behavior is attributed to the fact that, as pressure is increased, the discharge volume constricts into the 120-μm gap of the microstrip line. The constriction is shown in the photographs of Fig. 9. Because the constricted discharge has a much greater ratio of surface area to discharge volume, heat is readily transferred to the microstrip line and substrate. At low pressure, heat transfer to the substrate is the primary thermal loss mechanism. Nearer to atmospheric pressure, heat is also removed from the discharge zone by simple gas conduction and convection. These three mechanisms act to maintain the atmospheric pressure microplasma at or near room temperature [12].

V. Conclusion

The excitation, rotational, and vibrational temperature of an argon discharge with a 0.1% trace of nitrogen have been studied for a variety of pressure and power conditions by optical emission spectroscopy. The plasma source used in this paper is a low-power microwave plasma source based on a microstrip split-ring resonator similar to the one recently reported in [15]. This source has a much smaller discharge gap (120 μm versus

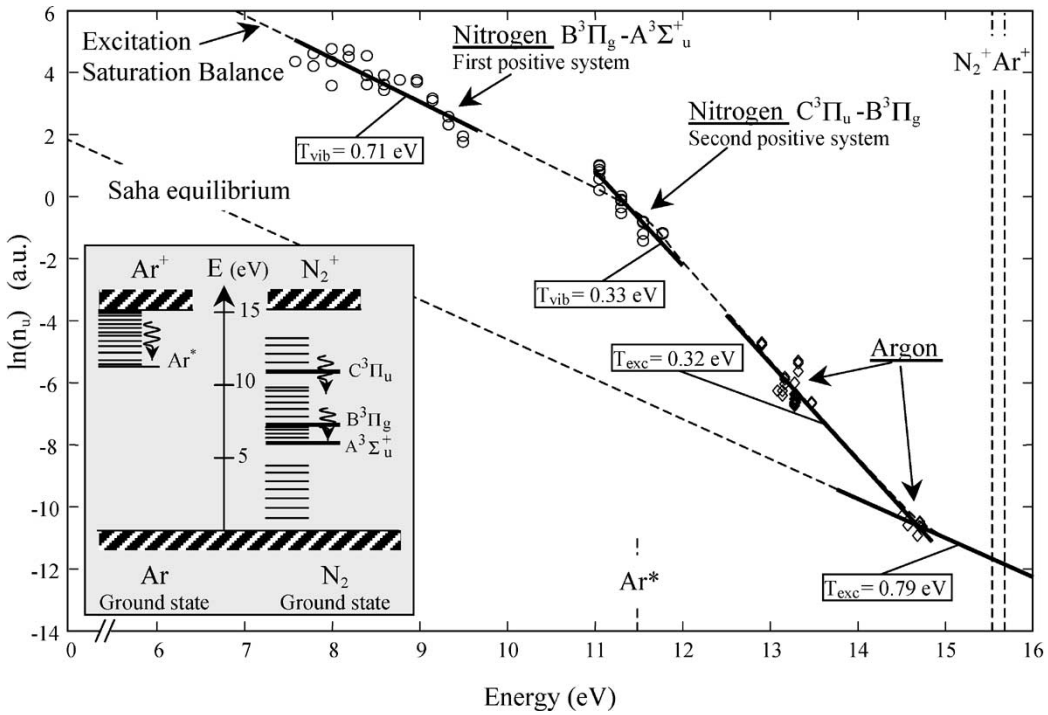

Fig. 7. Relative population of excited states $ln(n_u)$ is plotted as a function of energy in a 99.9% Ar–0.1% N_2 discharge at atmospheric pressure and 1 W.

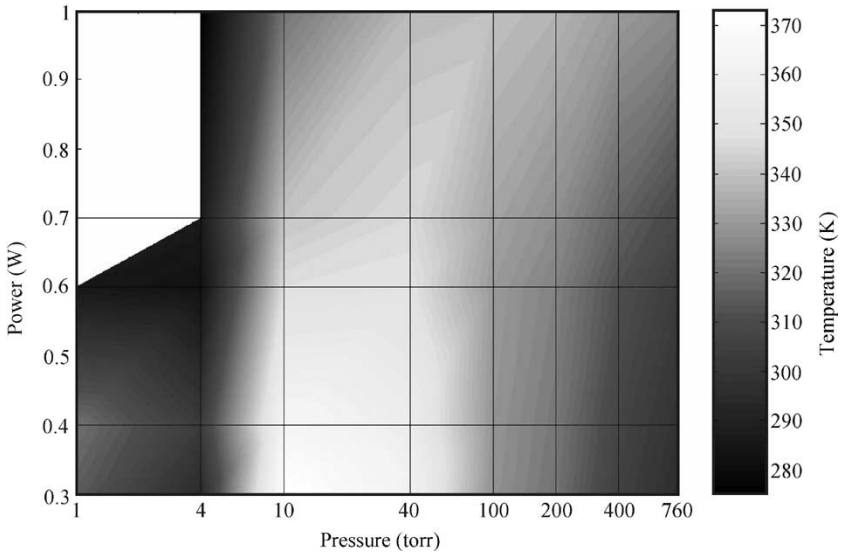

Fig. 8. Rotational temperature in a 99.9% Ar–0.1% N_2 discharge as a function of pressure and power. Rotational temperature is experimentally determined by fitting the $\Delta\nu = 0$, $\Delta\nu = 1$, and $\Delta\nu = 2$ sequences of the nitrogen second positive system.

Fig. 9. Microplasma operation in a 99.9% Ar–0.1% N_2 discharge at 0.3 W. (a) Discharge is relatively large and diffuse at 10 torr (1.3 kPa). (b) At atmospheric pressure the microdischarge is localized near the gap in the split-ring resonator.

500 μm), which improves the performance at high pressure, and its design eliminates the need for a matching network. Therefore, a more compact and yet more efficient device has been obtained.

The plasma generated with this device is clearly not in thermal equilibrium even at atmospheric pressure due to the different values measured for the excitation, vibrational, and rotational temperature. The population of the vibrational states and the excited atomic levels show a typical excitation saturation balance profile, i.e., overpopulation of low-energy levels due to the step-like excitation/ionization process.

The rotational temperature measurement shows that the discharge is hottest (∼400 K) at intermediate pressures (10–100 torr) for a given input power. The temperature at

atmospheric pressure, however, is around room temperature ($\sim$300 K) for input powers less than 1 W. So, although this discharge has intense optical emission reminiscent of an arc, the microwave microplasma is a nonthermal discharge that is well suited for low-power, portable applications.

REFERENCES

[1] J. C. T. Eijkel, H. Stoeri, and A. Manz, "A molecular emission detector on a chip employing a direct current microplasma," *Anal. Chem.*, vol. 71, pp. 2600–2606, 1999.

[2] J. C. T. Eijkel, H. Stoeri, and A. Manz, "A DC microplasma on a chip employed as an optical emission detector for gas chromatography," *Anal. Chem.*, vol. 72, pp. 2547–2552, 2000.

[3] C. G.Chester G. Wilson and Y. B.Yogesh B. Gianchandani, "Spectral detection of metal contaminants in water using an on-chip microglow discharge," *IEEE Trans. Electron Devices*, vol. 49, pp. 2317–2322, Dec. 2002.

[4] R. H. Stark and K. H. Schoenbach, "Direct current glow discharge in atmospheric air," *Appl. Phy. Lett.*, vol. 74, no. 25, pp. 3770–3772, 1999.

[5] P. Kurunczi, J. Lopez, H. Shah, and K. Becker, "Excimer formation in high-pressure microhollow cathode discharge plasmas in helium initiated by low energy electron collisions," *Int. J. Mass Spectrometry*, vol. 205, pp. 277–283, 2001.

[6] R. H. Stark, U. Ernst, R. Block, M. El-Bandrawy, and K. H. Schoenbach, "Microhollow cathode discharges in atmospheric air," in *Proc. 1999 IEEE Int. Conf. Plasma Science (ICOPS'99) IEEE Conf. Record—Abstracts*, 1999, p. 117.

[7] J. P. Boeuf, "Plasma display panels: Physics, recent developments and key issues," *J. Phys. D: Appl. Phys.*, vol. 36, pp. R53–R79, 2003.

[8] M. Laroussi, "Nonthermal decontamination of biological media by atmospheric-pressure plasmas: Review, analysis, and prospects," *IEEE Trans. Plasma Sci.*, vol. 30, pp. 1409–1415, Aug. 2002.

[9] J. G. Birmingham and D. J. Hammerstrom, "Bacterial decontamination using ambient pressure nonthermal discharges," *IEEE Trans. Plasma Sci.*, vol. 28, pp. 51–55, Feb. 2000.

[10] J. Ozonek, K. Jahołkowski, I. Pollo, and S. Okazaki, "Operation conditions in an ozonizer containing wire packing," in *Proc. Int. Symp. High Pressure, Low Temperature Plasma Chemistry, HAKONE VIII*, vol. II, Puhajarve, Estonia, 2002, pp. 239–243.

[11] H. Yoshiki and Y. Horiike, "Capacitively coupled microplasma source on a chip at atmospheric pressure," *Jpn. J. Appl. Phys.*, vol. 40, no. 4A, pp. L360–L362, Apr. 2001.

[12] E. Stoffels, A. J. Flikweert, W. W. Stoffels, and G. M. W. Kroesen, "Plasma needle: A nondestructive atmospheric plasma source for fine surface tratment of (bio)materials," *Plasma Sources Sci. Technol.*, vol. 11, pp. 383–388, 2002.

[13] A. M. Bilgic, U. Engel, E. Voges, M. Kuckelheim, and J. A. C. Broekaert, "A new low-power microwave plasma source using microstrip technology for atomic emission spectrometry," *Plasma Sources Sci. Technol.*, vol. 9, no. 1, pp. 1–4, Feb. 2000.

[14] A. M. Bilgic, E. Voges, U. Engel, and J. A. C. Broekaert, "A low-power 2.45 GHz microwave induced helium plasma source at atmospheric pressure based on microstrip technology," *J. Anal. Atomic Spectrometry*, vol. 15, no. 6, pp. 579–580, 2000.

[15] F. Iza and J. Hopwood, "Low-power microwave plasma source based on a microstrip split-ring resonator," *IEEE Trans. Plasma Sci.*, vol. 31, pp. 782–787, Aug. 2003.

[16] R. K. Hoffman, *Handbook of Microwave Integrated Circuits*. Norwood, MA: Artec House, 1987, p. 207.

[17] M. A. Lieberman and A. J. Lichtenberg, *Principle of Plasma Discharges and Materials Processing*. New York: Wiley, 1994, p. 96.

[18] J. A. M. van der Mullen, "Excitation equilibria in plasmas; A classification.," *Phys. Rep. (191)*, pp. 109–220, 1990.

[19] H. R. Griem, *Principle of Plasma Spectroscopy*. Cambridge, U.K.: Cambridge Univ. Press, 1997.

[20] A. R. Striganov and N. S. Sventitskii, *Tables of Spectral Lines of Neutral and Ionized Atoms*. New York: Plenum, 1968.

[21] F. R. Gilmore, R. R. Laher, and P. J. Espy, "Franck-Condon factors, r-centroids, electronic transition moments, and Einstein coefficients for many nitrogen and oxygen systems," *J. Phys. Chem. Ref. Data*, vol. 21, pp. 1005–1067, 1992.

[22] G. Herzberg, *Molecular Spectra and Molecular Structure*, 2nd ed. New York: Van Nostrand, 1950.

[23] J. A. Bittencourt, *Fundamentals of Plasma Physics*. New York: Pergamon, 1986, pp. 189–193.

Felipe Iza (S'03) received the B.S. degree in engineering from the University of Navarra, San Sebastian, Spain, in 1997, and the M.S. degree from Northeastern University, Boston, MA, in 2001, where he is currently working toward the Ph.D. degree.

From 1997 to 1999, he was with the Centro de Estudios e Investigaciones Tecnicas de Guipuzcoa (CEIT), San Sebastian, Spain. His current areas of interest include MEMS and microplasmas. He has researched microfabricated inductively coupled plasma sources operating at radio frequencies and is currently developing new sources to investigate submillimeter scale plasmas generated at microwave frequencies and their integration in MEMS systems.

Mr. Iza is a student member of the American Vacuum Society.

Jeffrey A. Hopwood (S'86–M'90) received the Ph.D. degree in electrical engineering from Michigan State University, East Lansing, in 1990.

He was with the T. J. Watson Research Center, the IBM Corporation, Yorktown Heights, NY, until 1993. He is currently an Associate Professor of electrical and computer engineering with Northeastern University, Boston, MA. His research interests are focused on plasma generation and plasma processing, and include microplasma generation, micromachining of challenging materials, plasma deposition of microelectronic interconnects, and plasma-enhanced atomic layer deposition.